APPLICATION OF THE LIFTING LINE CONCEPT TO HELICOPTER COMPUTATION

by Jean-Joël COSTES

Office National d'Etudes et de Recherches Aérospatiales (ONERA)
92320 Châtillon (France)

SUMMARY

This paper presents some comparisons between theory and experiment for the lifting force on the blade of a model of helicopter in forward flight. It is shown that the accuracy of the results obtained by the lifting line method decreases for high advance ratio flights, especially at the blade tip. The coupling of 3-D and skewed flow effects, added to unsteady aerodynamics which occurs there, is studied on a simplified model.

APPLICATION DU CONCEPT DE LIGNE PORTANTE
AUX CALCULS D'HÉLICOPTÈRES

RÉSUMÉ

Dans cet article, on présente des comparaisons entre la théorie et l'expérience pour la portance d'une pale de maquette d'hélicoptère en vol avançant. La précision des résultats diminue lorsque le rapport d'avancement augmente, en particulier pour l'extrémité libre de la pale. L'interaction des effets tridimensionnels et instationnaires, ajoutée aux conséquences d'une attaque oblique qui se produit en cet endroit, est étudiée sur un modèle simplifié.

INTRODUCTION

Even with the advent of fast computers, calculation time is still a severe limitation in helicopter aerodynamics. On this field the acceleration potential theory associated with the lifting line concept has proved to be a successful method. Nevertheless, simplifications and computer time saving cannot be introduced without any drawbacks. This paper is a contribution to the study of unsteady aerodynamics on the helicopter blade, especially at the tip of the advancing blade where three-dimensional and skewed flow effects are added

I. USE OF THE ACCELERATION POTENTIAL THEORY IN LIFTING SURFACE CALCULATION

1. General assumptions and equations

A compressible non viscous fluid is at rest while a body is moving at velocity $V(t)$ through it. This body induces small perturbations in the fluid, and its acceleration may be derived from a potential ψ. By neglecting the second order terms, the potential $\psi(P, t)$ at a point P and time t is governed by the following equation (conservation of mass) :

(1)
$$\frac{\partial^2 \psi}{\partial x^2} + \frac{\partial^2 \psi}{\partial y^2} + \frac{\partial^2 \psi}{\partial z^2} - \frac{1}{a^2}\frac{\partial^2 \psi}{\partial t^2} = 0$$

a : is the velocity of sound into the fluid.

The momentum equation gives a relation between the pressure and the potential ψ :

(2)
$$\psi = \frac{-[p - p_\infty]}{\rho_\infty}$$

p_∞ is the pressure of the unperturbed fluid,
ρ_∞ is the density of the fluid at infinity.

The potential ψ must satisfy some boundary conditions, such as zero at infinity, and also fulfil non separation conditions on the surface of the body. Due to the linearisation, a velocity potential may be obtained by integration over the time variable :

(3)
$$\varphi(P, t) = \int_{-\infty}^{t} \psi(P, \tau)\, d\tau$$

Derivations of the velocity potential $\varphi(P, t)$ with respect to the space variables are used to satisfy the non-separation condition.

2. Application to lifting surface computations

In all the following, thickness effects are neglected.

This simplification allows the use of the particular solution given by the doublet potential which is particularly suited for lifting surface problems. Thus if a lifting surface $\mathscr{S}$ (fig. 1) has a surface distribution of doublet of strength $q(P_0, t)$ and axis normal to $\mathscr{S}$, then the pressure jump across $\mathscr{S}$ is related to $q(P_0, t)$ by the formula :

(4)
$$q(P_0, t) = \frac{[p^+(P_0) - p^-(P_0)]}{\rho_\infty}$$
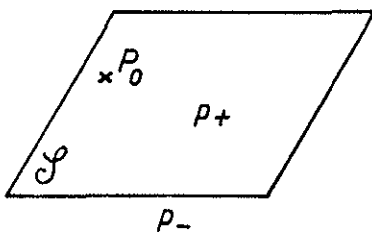
Fig. 1 — Lifting surface $\mathscr{S}$.

The potential induced in the open space by a moving doublet has been determined for a compressible fluid in [1]. The acceleration potential $\psi(P, t)$ created at the point P and time t by a doublet placed at point P_0 and time τ is :

(5)
$$\psi(P, t) = \frac{dq(\tau)}{d\tau}\frac{\vec{n_0}.\vec{D}}{-4\pi |D|^2 a\, r_0^2} + \frac{q(\tau)(\vec{D}.\vec{V_0})(\vec{n_0}.\vec{D})}{-4\pi a^2 |D|^3\, r_0^3} + q(\tau)\frac{\frac{d\vec{n_0}}{d\tau}.\vec{D}}{-4\pi|D|^2 a\, r_0^2}$$

$$+ q(\tau)\frac{[(a^2 - |V_0|^2)(\vec{n_0}.\vec{D}) + (\vec{V_0}.\vec{D} - a|D|)(\vec{V_0}.\vec{n_0})]}{-4\pi a^2 |D|^3\, r_0^3}$$
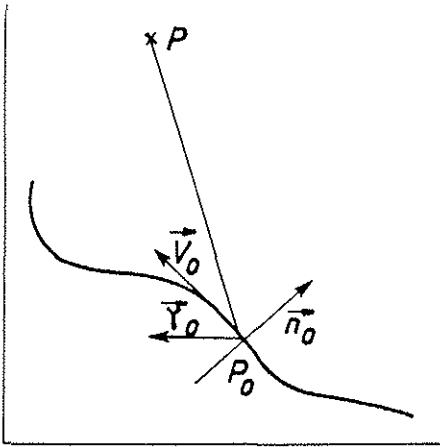
Fig. 2 — Moving doublet.

where (fig. 2)

$$\vec{D} = \overline{P_0 (\tau) P} \quad and \quad \tau_0 = \left[1 - \frac{\vec{V_0} . \vec{D}}{a \, |D|} \right]$$

$q(\tau)$ is the doublet intensity at time τ

$\frac{dq(\tau)}{d\tau}$ is the derivative with respect to the time variable

$\vec{V}(\tau)$ is the velocity of the doublet at time τ

$\vec{\gamma}(\tau)$ is the acceleration of the doublet at time τ

$\vec{n_0}(\tau)$ is the direction of the doublet axis at time τ

τ is determined by the relation :

(6) $$\tau = t - \frac{|D|}{a}$$

Formula (5) satisfies equation(1) and is used for lifting surface computation with a doublet axis normal to the wake $(\vec{V_0}.\vec{n_0}) = 0$ this is a consequence of the usual linearisation assumption where the lifting surface is projected over the wake surface. The non separation condition is replaced by a relation giving the value of the projection of the fluid velocity onto the local normal to the wake. At any point P the fluid acceleration is obtained by a summation over the whole lifting surface (equation(1) is linear) with the appropriate doublet intensity. According to (3) the velocity potential is ·

(7) $$\varphi(P,t) = \iint_{\mathcal{S}} \int_{-\infty}^{\tau_1(P_0)} \left[\frac{-\frac{d[q\vec{n_0}].\vec{D}}{d\tau}}{4\pi a \, |D|^2 \tau_0^2} + \frac{-q(\tau)(\vec{D}.\vec{\gamma_0})(\vec{n_0}.\vec{D}) + (a^2 - \vec{V_0}^2)(\vec{n_0}.\vec{D})}{4\pi a^2 \, |D|^3 \tau_0^3} \right] d\sigma d\tau$$

This formula may also be used in the equivalent form

(8) $$\varphi(P,t) = \iint_{\mathcal{S}} \frac{-q(P_0, \tau_1)[\vec{n_0}(\tau_1).\vec{D}(\tau_1)]}{4\pi a \, |D|^2 \tau_0(\tau_1)} d\sigma + \iint_{\mathcal{S}} \int_{-\infty}^{\tau_1} \frac{-q(P_0, \tau)[\vec{n_0}.\vec{D}]}{4\pi \, |D|^3} d\sigma d\tau$$

where $$t - \tau_1 = \frac{|D(P_0, \tau_1)|}{a}$$

Relation (8) can be derived from (7) using integration by parts or may be obtained directly as in |2|.

Due to the limitations on computer time, equations (7) or (8) involving a surface integral are simplified everytime the lifting surface can be approximated by a lifting line. This is the case for a helicopter blade in the calculations presented in this paper. When a single line approximates the blade, it is placed on the 25 % chord position. Equation (8) then becomes :

(9) $$\varphi(P,t) = \int_{R_0}^{R_1} \frac{F(\pi, \tau_1)[\vec{n_0}.\vec{D}]}{4\pi \rho_\infty a \, |D|^2 \tau_0(\tau_1)} d\pi + \int_{R_0}^{R_1} \int_{-\infty}^{\tau_1} \frac{F(\pi, \tau)[\vec{n_0}.\vec{D}]}{4\pi \rho_\infty \, |D|^3} d\pi d\tau$$

The lifting line is described by the parameter π taking values between R_0 and R_1

$$R_0 \leq \pi \leq R_1$$

$F(\pi, \tau)$ is the lifting force per unit length and is related to the doublet intensity by the relation of the same kind as (4)

$$(10) \qquad q(\tau, \zeta) = - \frac{F(\tau, \zeta)}{\rho_\infty}$$

3. Research of a formulation suitable for problems in aeroelasticity

In a great number of practical problems, such as the computation of aerodynamic forces on a helicopter blade, the lifting surface movement depends on the aerodynamic forces, which in turn are determined by the lifting surface displacements through the non separation condition. One must solve two sets of simultaneous equations. The first set expresses the mechanical behaviour of the blade (elasticity equation), the second set is derived from equation (9). For a complete problem, the computation time may become quite large and is likely to be carried out on a limited number of selected blade movements or for a limited number of different lift distributions. Making use of the linear character of the problem, one should be able to obtain the solution satisfying some particular conditions. In this paper, in addition to the single lifting line approximation, the lift force is decomposed on a polynomial basis along the blade span combined with a Fourier series development for the time variable. The problem is thus restricted to established periodical forces and blade movements.

$$(11) \qquad F(\tau, t) = \sqrt{1 - \eta^2} \left[\sum_{i=1}^{n} \mathcal{Z}_i L_i(\tau) + \sum_{i=1}^{n} \sum_{j=1}^{m} X_{ij} \cos j\Omega t \, L_i(\tau) \right.$$
$$\left. + \sum_{i=1}^{n} \sum_{j=1}^{m} Y_{ij} \sin j\Omega t \, L_i(\tau) \right]$$

where $\eta = \dfrac{2\tau - R_1 - R_0}{R_1 - R_0}$

In expression (11) the factor $\sqrt{1 - \eta^2}$ makes $F(\tau, t)$ zero at both ends of the blade. The $L_i(\tau)$ are Lagrange polynomials. The $\mathcal{Z}_i$, X_{ij} and Y_{ij} are the coefficients of the decomposition of $F(\tau, t)$. The $\mathcal{Z}_i$, X_{ij}, Y_{ij} are to be determined by substituting (11) in equation (9); the velocity potential may be determined at every point in space. For the helicopter problem, the blade wake (fig. 3) may be
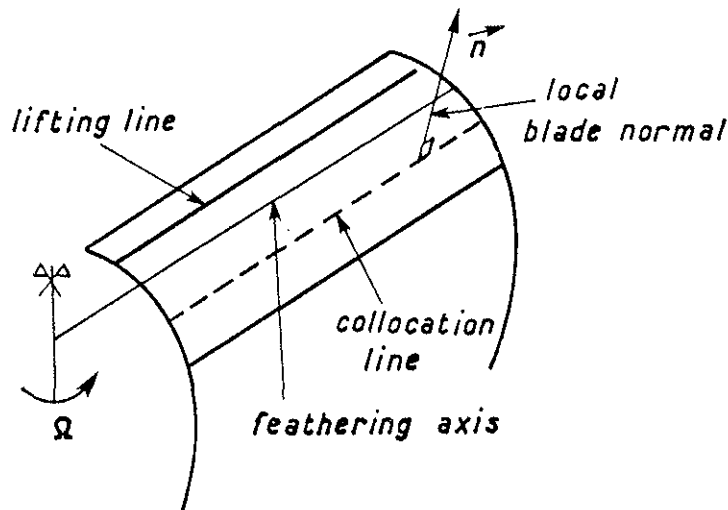
Fig. 3 — Helicopter blade wake.

considered to be generated by the feathering axis rotating and translating through space. The blade surface is projected on the wake and the single lifting line occupies the 25 % chord position. As for the classical wing problem, the non separation condition is satisfied on a line situated at the 75 % chord position. In fact, due to the limited

number of Lagrange polynomials, the non separation condition is expressed only at n spanwise positions x_i such that $L_i(x_i) = 1$. The velocity potential is computed for two points on the normal of the blade and the velocity is obtained by finite difference. The non separation condition is expressed at some $(2m + 1)$ instants t_j to furnish the whole set of aerodynamic equations. When the blade movement is known, this set of equations is sufficient to determine the lift force coefficients. In case of an unknown blade movement, the blade must be modelised by a set of mechanical equations [4]

II. APPLICATION TO A HELICOPTER ROTOR IN ADVANCING FLIGHT

A helicopter rotor model has been built by the Société Aérospatiale (SNIAS) and extensive tests were carried out in Modane during July 1970. The model is a three-bladed, falp-and-lag articulated rotor with fairly stiff blades. The blades are instrumented with pressure transducers in four sections at spanwise positions x/R = 0.52 ; 0.71 ; 0.855 ; 0.952. Blade movements were recorded during the experiments and can be used as input parameters if necessary. Two comparisons between theory and experiment are presented, the first for an advance ratio of μ= 0.3 and the second μ = 0.44

1. Comparison between theory and experiment for an advance ratio of μ= 0.30

There was no stall in the presented flight case, so the linear theory is valid. Two computations have been done. First of all, the recorded blade movement is used as an input and the aerodynamic forces are compared with the experiment. Then the blade which is assumed to be rigid is characterised by its various inertia properties (moments of inertia, position of the center of mass etc....) and the set of mechanical equations is introduced.

Again the aerodynamic forces are compared with the experiment.

Results for both cases are presented in figures 4 a, b, c, d in a non dimensional form :

$$P_m(t) = \int_{chord} \frac{\Delta p(t)}{P_0} \, d\left(\frac{x}{c}\right)$$

P_0 is the static pressure in the wind tunnel .

a) r/R = 0.520

b) r/R = 0.710
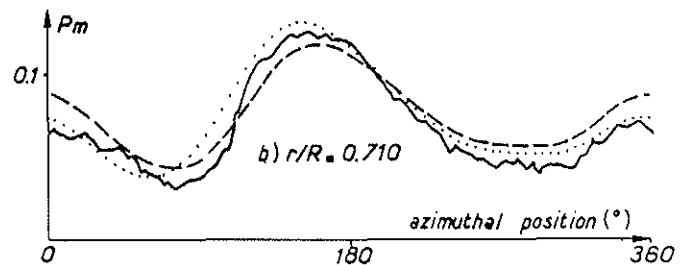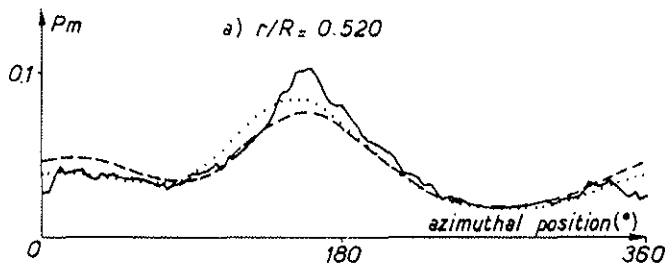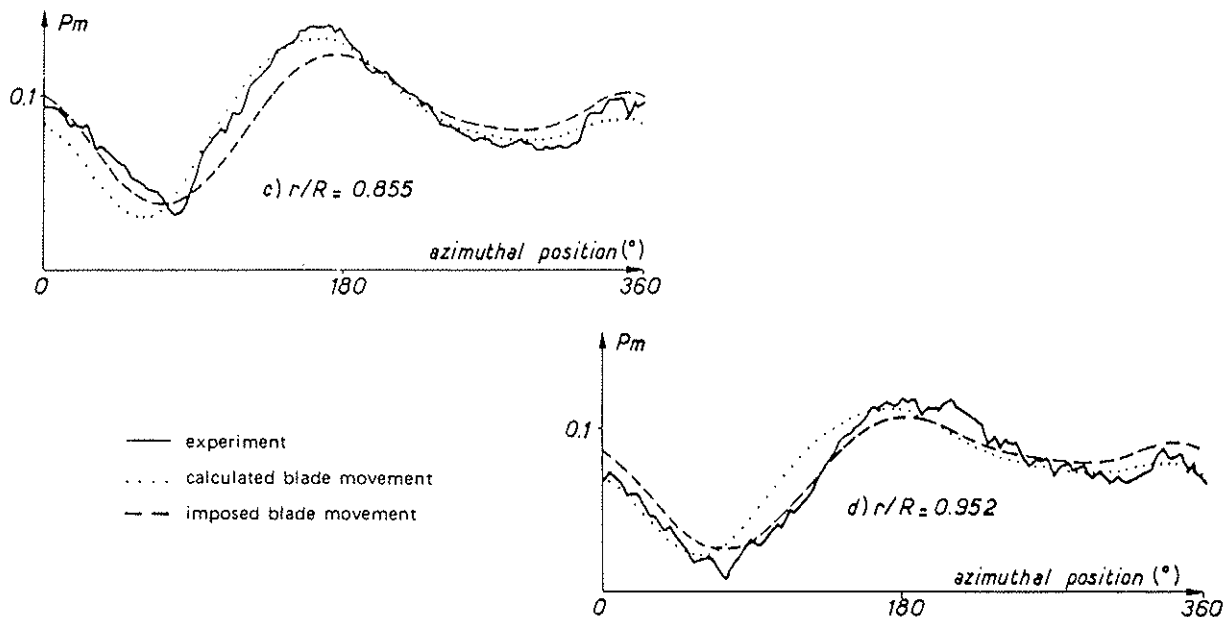
Fig. 4 (a, b, c, d) — Time history of the lifting force. Comparison between theory and experiment at advance ratio $\mu = 0.30$

Though both results agree rather well with the experiment, some curious phase shifts seem to appear and discrepancies can be large for the advancing blade at azimuthal angles between $90°$ and $180°$. This phenomenon is easily seen in figure 5 where the experimental blade movement is taken as an input in the calculations. Agreement is good except for the first cosine term where the predicted level is too low. The origin of this discrepancy may be a systematic error in the prediction of unsteady forces by a single lifting line or a swept flow effect. These two points will be examined on the next paragraphs.

A_i = cosine part of rank i

B_i = sine part of rank i
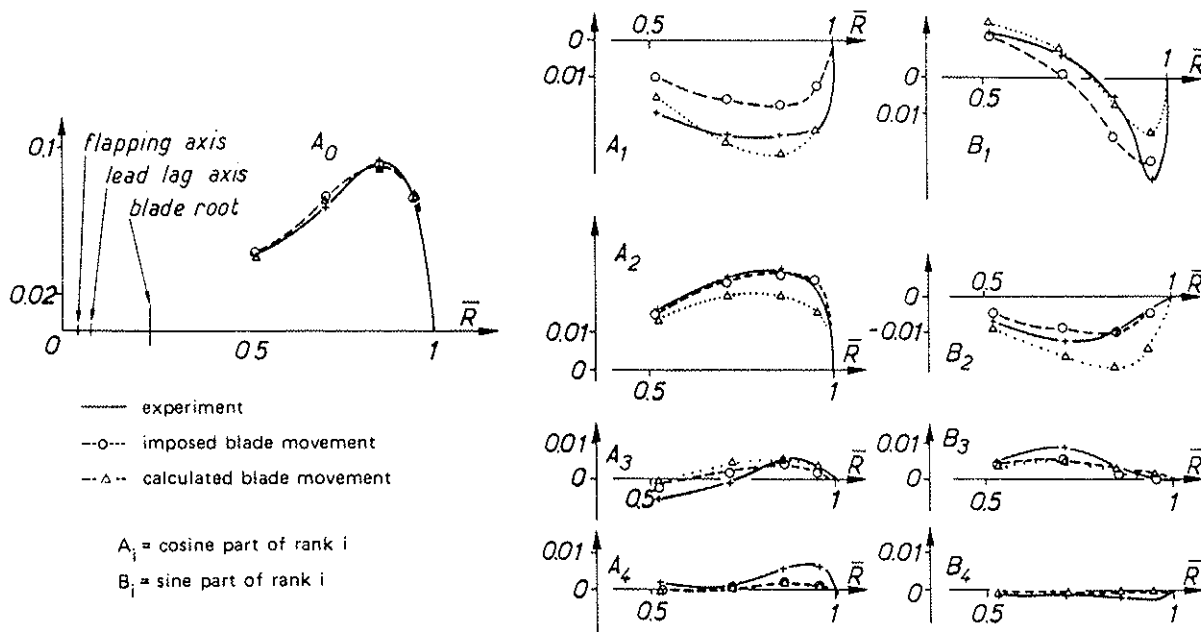
Fig. 5 — Harmonic analysis of the lifting force : $\mu = 0.3$; $\alpha_Q = -16°$

2. Comparison at an advance ration μ = 0.44

Results are given in figures 6 a, b, c, d. The blade movement has been computed. Some important discrepancies are now occurring, particularly for the advancing blade azimuthal region.

This phenomenon will be studied in paragraph IV for a simplified case.
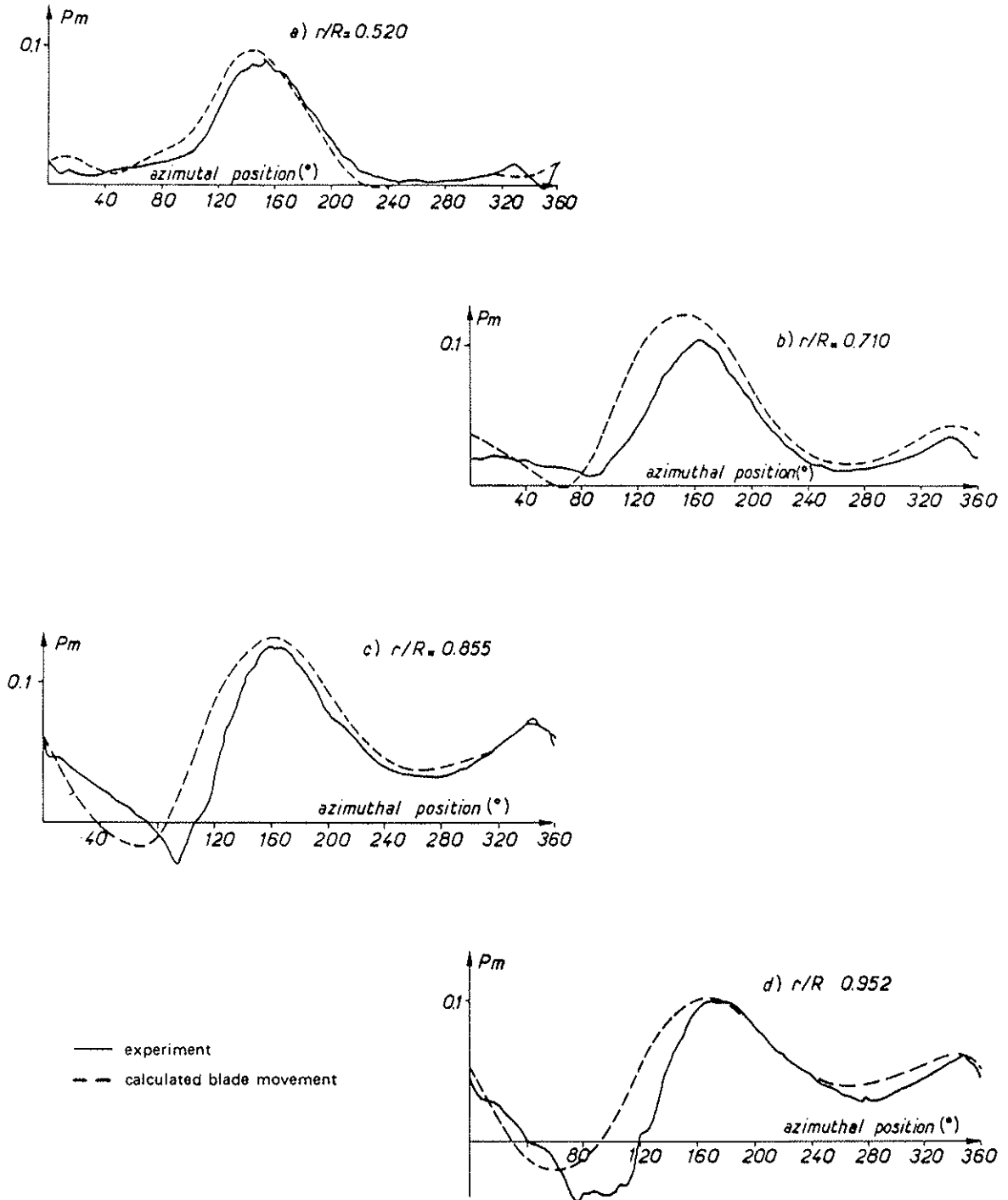
Fig. 6 (a, b, c, d) — Time history of the lifting force. Comparison between theory and experiment at advance ratio μ = 0.44

III. UNSTEADY EFFECT ON THE LIFTING LINE APPROXIMATION

The effect of unsteady motion is particularly simple to study in two dimensional incompressible flow. Results can be compared with Theodorsen's theory for the flat plate [6].

1. Downwash computation
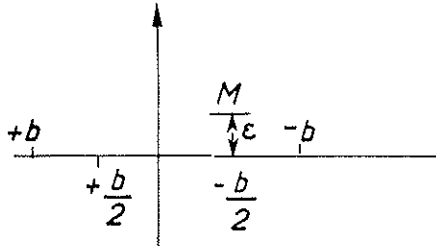
Fig. 7 — 2-D moving doublet.

A 2-D doublet is moving with a constant velocity V through an incompressible fluid (fig. 7). This doublet is supposed to schematise a profile. At instant $t = 0$, the positions of the profile is :

At the same instant $t = 0$, the position of the doublet is $y = +\frac{b}{2}$ and the downwash velocity is computed at point $M\left(x = \varepsilon, \; y = -\frac{b}{2}\right)$

The parameter ε is small and will eventually be zero. The lifting force on the profile is periodical and takes the form : $F(t) = F_0\, e^{j\,2\pi f t}$ The potential at the point M is given at time $t = 0$ by :

(12)
$$\varphi(M, t=0) = \int_{-\infty}^{0} \frac{F_0\, e^{j\,2\pi f \tau}\, \varepsilon\, d\tau}{2\pi \rho_\infty\left([V\tau + b]^2 + \varepsilon^2\right)}$$

Taking $u = -\dfrac{V\tau}{b}$ and introducing the reduced frequency $k = \dfrac{2\pi f b}{V}$ the relation (12) becomes :

(13)
$$\varphi(M, t=0) = \frac{F_0}{2\pi \rho_\infty V} \int_{0}^{+\infty} \frac{\varepsilon^*\, e^{-j\,ku}}{[1-u]^2 + \varepsilon^{*2}}\, du$$

where $\varepsilon^* = \dfrac{\varepsilon}{b}$

The downwash is obtained by derivation with respect to ε. Then ε is made to be zero, which gives :

(14)
$$v(M, t=0) = \frac{F_0}{2\pi \rho_\infty V b} \oint_{0}^{+\infty} \frac{e^{-j\,ku}}{(1-u)^2}\, du$$

The integral (14) is singular for $u = 1$, but may be integrated using integral sine and cosine functions ; one obtains :

(15)
$$v(M, t=0) = \frac{F_0}{2\pi \rho_\infty V b} \left[-1 + k\, e^{-j\,k} \left[j\, C_i(k) - \frac{\pi}{2} + S_i(k) \right] \right]$$

where
$$C_i(k) = -\int_{k}^{+\infty} \frac{\cos v}{v}\, dv \quad ; \quad S_i(k) = \int_{0}^{k} \frac{\sin v}{v}\, dv$$

2. Non separation condition and results

The profile is oscillating with amplitude α and frequency f around a center of rotation at ordinate $y = \xi$. A vertical translation with amplitude h and frequency f is added to the preceding movement. The velocity at point M and instant t is given by :

$$\text{(16)} \qquad v(M, t) = j\, 2\pi f \left[h + \left(\xi + \frac{b}{2} \right) \alpha \right] - \alpha V$$

By combination of (15) and (16), the complex number F_v may be obtained, giving amplitude and phase of the lifting force.

Two cases are examined :

1) a pure oscillatory movement around $y = \dfrac{b}{2}$,

2) a pure vertical translation.

In figures 8 and 9, results are compared with the exact Theodorsen's theory for a flat plate. Phase angles are given with respect to the profile movement.
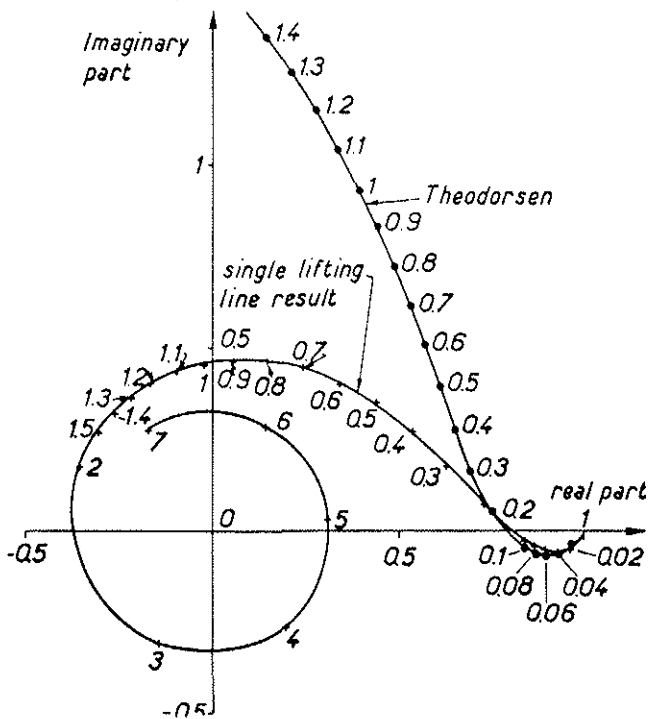
Fig. 8 — Oscillatory motion around y = b/2.

Lifting force is given by its real and imaginary parts which are to be multiplied by 2 $\pi \rho b V^2 \alpha$.

Curves are graduated in reduced frequencies k = 2 $\pi f b/V$.
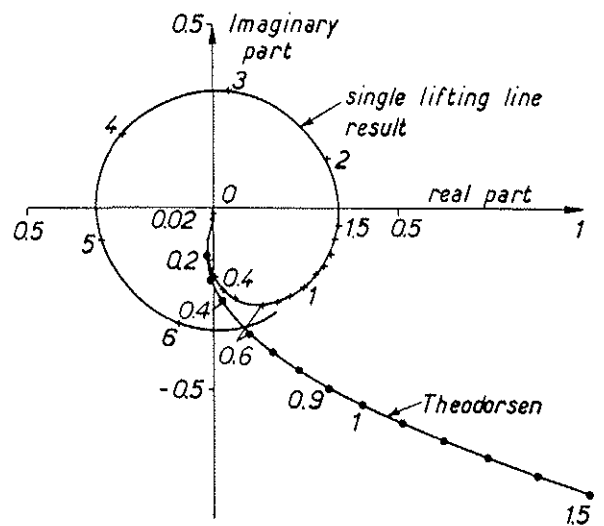
Fig. 9 — Vertical translation.

Lifting force is given by its real and imaginary parts which are to be multiplied by 2 $\pi \rho V^2 h$.

Curves are graduated in reduced frequencies k = 2 $\pi f b/V$.

For both cases, at reduced frequency $k = 0$, lifting line results are the same as Theodorsen's results. In fact, the relative position of the lifting point and the collocation point are chosen for such an agreement. With increasing frequency, some discrepancies occur, but agreement is very good up to $k = 0.2$. In the Theodorsen's theory the lifting force keeps increasing with frequency. This is not the case in lifting point computation where the force tends toward zero. For a compressible flow the behaviour of the lifting force is preserved, as shown in figure 10. A possibility to improve the results is to increase the number of lifting lines; the improvement with five lifting lines is quite substantial, but results are still far from the exact ones given by the lifting surface theory (fig. 10).

To have an idea of the reduced frequencies encountered on a helicopter blade, they have been computed for the SA349 (Gazelle) SNIAS helicopter. The lifting surface of the blade is rectangular ; the spanwise position is such that $1.523 \leqslant r \leqslant 5.073$ m ; the chord is 0.35 m.
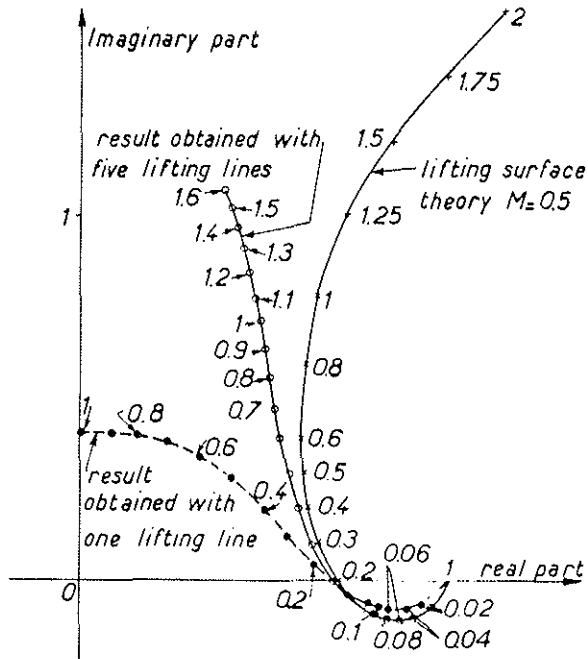
Fig. 10 — Oscillating motion around y = b/2

Lifting force is given by its real and imaginary parts

which are to be multiplied by $2\ \pi\rho V^2 a/\sqrt{1 - M^2}$.

Curves are graduated in reduced frequencies k = 2 πfb/V.

Mach number M = 0.5

the reduced frequencies computed at various spanwise locations $\mathcal{R}$ for the rotation frequency are :

$$\mathcal{k} = 0.046 \text{ at } \mathcal{R} = 0.75 \text{ R1}$$
$$\mathcal{k} = 0.069 \text{ at } \mathcal{R} = 0.5 \text{ R1}$$
$$\mathcal{k} = 0.114 \text{ at } \mathcal{R} = \text{R0}$$

with R0 = 1.523 and R1 = 5.073 m.

For a helicopter, as shown here, the reduced frequencies are quite low and the lifting line approximation is not a limitation .

IV. THREE-DIMENSIONAL EFFECT ON THE ADVANCING HELICOPTER BLADE
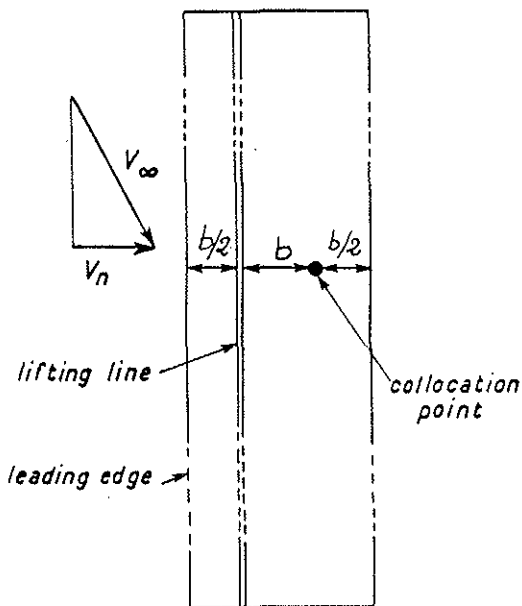
Fig. 11 — Rectangular blade of infinite length in swept flow.

For a rectangular blade of infinite length in a skewed incompressible flow (fig. 11), the unsteady downwash is still given by formula (15) as in normal attack, except for the replacement of V_∞ by V_n, the projection of V_∞ on a normal to the blade axis. Thus the behaviour of an actual helicopter blade in forward flight needs only to be studied in the tip region where three-dimensional and skewed flow effects are added. A simpler problem will be examined, the rectangular wing in skewed flow, which presents the same aerodynamic character as the actual advancing blade.

1. Rectangular wing in swept flow

Some simplifications are to be made. The wing is schematised by lifting lines with equal spacing chordwise. Furthermore on a lifting line the force is given by a step function. The position of the collocation points must be carefully chosen to avoid the effects of the abrupt variation of force on the lifting lines. These
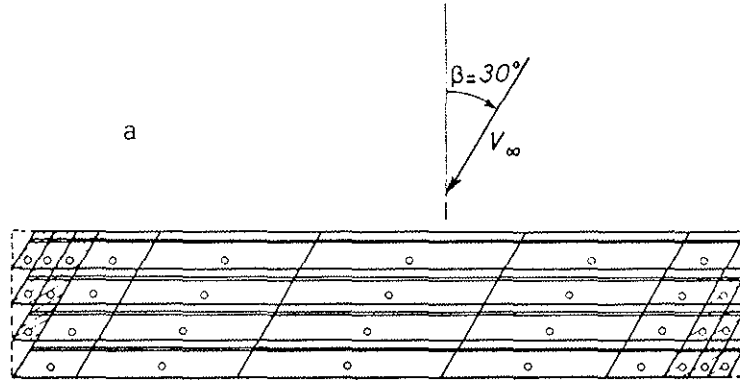
Fig. 12a — Approximation of a rectangular wing by an array of parallelograms,
whose spanwise dimension can be arbitrarily chosen, except in the two shaded areas.
b — Isolated parallelogram.
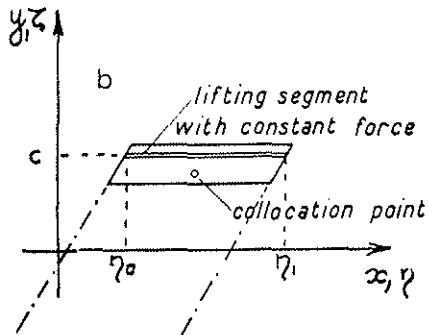
considerations lead to the blade schematisation of figure 12a, where the wing is cut into elements. The planform of these elements (fig. 12b) is a parallelogram, two sides being parallel to the velocity V_∞. The other two opposite sides are parallel to the wing span axis. Each of these elements is provided with a lifting segment and a collocation point. The lifting force is constant on the element and the lifting segment is fixed at the usual 25% chordwise position. The collocation point is at the 75% chordwise position and in the middle of the element spanwise. The elements are all of the same dimension chordwise, but their size can be different in the spanwise sense. Some elements (see fig. 12a) at both wing ends have their spanwise dimension given by the following formula :

(17)
$$d = \frac{c}{N}\, tg\, \beta$$

where d is the spanwise dimension,

c is the rectangular wing chord,

N is the number of elements chordwise,

β is the angle between the wind velocity and the wing span axis.

As shown by formula (17) the elements at the wing ends can be very thin when angle β is small ; this leads to mathematical difficulties discussed in the following section.

2. Calculation of the downwash induced by a lifting segment in a skewed incompressible flow

One isolated element, schematised by its lifting segment as in figure 12b, is considered. The segment induces, at any point P of the wing plane, a downswash velocity which is calculated here. A rectangular coordinate system (x , y) or (η , ζ) is used for the definition of the wing plane (fig. 12). At time $t = 0$, the coordinates of both extremities of the lifting segment are :

$$x = \eta_0 \ , \ y = c \quad \text{and} \quad x = \eta_1 \ , \ y = c$$

The two components of the velocity V_∞ are V_x and V_y. The potential in an incompressible flow is calculated at the distance $\mathcal{E}$ over the point $P(x, y)$ and is given by :

$$(18) \qquad \varphi(P, t=0) = \frac{1}{4\pi\rho_\infty} \int_{\tau=-\infty}^{\tau=0} F\, e^{j\nu\tau}\, d\tau \left\{ \int_{\eta_0}^{\eta_1} \frac{\mathcal{E}\, d\eta}{\left[(x-\eta-V_x\tau)^2 + (y-c-V_y\tau)^2 + \mathcal{E}^2\right]^{3/2}} \right\}$$

where the value of the force per unit length on the lifting segment is $F\, e^{j\nu\tau}$. By integration with respect to the variable η , (18) becomes :

$$(19) \qquad \varphi(P, t) = \frac{1}{4\pi\rho_\infty} \int_{-\infty}^{\tau=0} F\, e^{j\nu\tau} \left[G(x, y, \eta_1, \tau) - G(x, y, \eta_0, \tau) \right] d\tau$$

where

$$G(x, y, \eta, \tau) = \frac{-\mathcal{E}}{(y-c-V_y\tau)^2 + \mathcal{E}^2} \left[\frac{x-\eta-V_x\tau}{\left[(x-\eta-V_x\tau)^2 + (y-c-V_y\tau)^2 + \mathcal{E}^2\right]^{1/2}} \right]$$

Now, deriving with respect to $\mathcal{E}$ and making $\mathcal{E} = 0$, the downwash is given by :

$$(20) \qquad \sigma(P, t) = \frac{1}{4\pi\rho_\infty} \int_{-\infty}^{\tau=0} F\, e^{j\nu\tau} \left[\frac{\partial G}{\partial \mathcal{E}}(x, y, \eta_1, \tau) - \frac{\partial G}{\partial \mathcal{E}}(x, y, \eta_0, \tau) \right]_{\mathcal{E}=0} d\tau$$

where

$$\left[\frac{\partial G}{\partial \mathcal{E}}(x, y, \eta, \tau) \right]_{\mathcal{E}=0} = \frac{-1}{(y-c-V_y\tau)^2} \left[\frac{(x-\eta-V_x\tau)}{\left[(x-\eta-V_x\tau)^2 + (y-c-V_y\tau)^2\right]^{1/2}} \right]$$

Relation (20) is a Fourier Transform, and one is tempted to use a Fast Fourier Transform algorithm when numerical results are needed. Nevertheless this is not possible because of the singular part of $(\partial G)/(\partial \mathcal{E})$. The function $Y(\tau) = y - c - V_y\tau$ is zero for some value of the time τ. This singularity has already been encountered in the 2-D case (eq. 14) and the Fourier Transform of $\frac{1}{[Y(\tau)]^2}$ may be given using the integrals sine and cosine functions. One may then remove the singular part and now use the FFT algorithm. In fact the results will be good if the new function is smooth enough. This is the case except when the term

$$D(\tau) = \left[(x-\eta-V_x\tau)^2 + (y-c-V_y\tau)^2\right]^{1/2}$$ is very small. $D(\tau)$ cannot be zero because the collocation points P are by definition taken out of the paths of the lifting segment extremities. Nevertheless they may be small for some values of τ when the spanwise length of the element is small ; this occurs for a small angle β . Then it is necessary to subtract some other function to remove the remaining quasi-singular part. This function must have a good behaviour at infinity, on easily computable Fourier Transform, and match the desired function when $D(\tau)$ is small. Such a function exists and is not unique ; in this paper the following one has been chosen :

(21) $\quad H(\tau) = \dfrac{0.5}{X(\tau)^2 + \alpha\, Y(\tau)^2}$ $\qquad$ where : $\quad X(\tau) = x - \eta - V_x\tau$ $\qquad$ and $\quad \alpha = \dfrac{1}{\sqrt{2}}$

the Fourier transform of $H(\tau)$ can be expressed with the complex integral exponential functions (see Annex A).

The downswash of relation (20) will be calculated in the following way :

taking :

$$\frac{\partial G_1}{\partial \varepsilon}(x, y, \eta, \tau) = \frac{-X(\tau)}{Y(\tau)\left[X(\tau)^2 + Y(\tau)^2\right]^{1/2}} + Sgn\left[X^*(\eta)\right]\left[\frac{1}{Y(\tau)} - \frac{0.5}{X^2(\tau) + \alpha\, Y(\tau)^2}\right]$$

where $\quad X^*(\eta) = x - \eta - \dfrac{V_z}{V_y}(c - y)$

$\qquad$ and $\quad Sgn\,(X^*) = +1 \ \ if \ \ x^* > 0$

the relation (20) becomes :

$\qquad\qquad\qquad\qquad Sgn\,(x^*) = -1 \ \ if \ \ x^* < 0$

(22)

$$\sigma(P, t) = \frac{1}{4\pi\rho_\infty}\int_{-\infty}^{\tau=0}\left[\frac{\partial G_1}{\partial \varepsilon}(x, y, \eta_1, \tau) - \frac{\partial G_1}{\partial \varepsilon}(x, y, \eta_0, \tau)\right] F\, e^{j\nu\tau}\, d\tau$$

$$-\frac{1}{4\pi\rho_\infty}\int_{-\infty}^{\tau=0} F\, e^{j\nu\tau}\left[Sgn\left(X^*(\eta_1)\right) - Sgn\left(X^*(\eta_0)\right)\right]\frac{1}{Y(\tau)}\, d\tau$$

$$+\frac{1}{4\pi\rho_\infty}\int_{-\infty}^{\tau=0}\frac{1}{2} F\, e^{j\nu\tau}\left[\frac{Sgn\left(X^*(\eta_1)\right)}{X_1^2(\tau) + \alpha\, Y(\tau)^2} - \frac{Sgn\left(X^*(\eta_0)\right)}{X_0^2(\tau) + \alpha\, Y(\tau)^2}\right] d\tau$$

where $X_1(\tau) = x - \eta_1 - V_x\tau$ $\qquad$ and $\quad X_0(\tau) = x - \eta_0 - V_x\tau$

In this formula the first integral is numerically computed by means of the FFT algorithm ; the other two integrals are expressed with the integrals sine cosine and exponential functions.

3. Presentation of some results

The downswash of formula (22) is used to express the non separation condition at the collocation points of the wing. Some computations have been done in the case of a wing with a constant incidence. First of all, for the wing of figure 12a the forces on each lifting segment have been obtained for a stationary case (reduced frequency $k = 0$). The results are given in figure 13. One of the wing ends behaves like a leading edge, and thus the forces are increasing in this region. This fact is easily noticeable on the lifting line close to the wing trailing edge, the forces being small there.

For an angle $\beta = 1°$ the elements at both extremities of the wing are very thin, and could have been neglected. They are almost degenerated, but with the introduction of the Fourier Transform of $H(\tau)$ the results remain good (see fig. 14). The lift is still increasing at the leading tip, but the lifting segments are very short and the contributions to the overall force can be almost neglected. The lifting force decreases at both ends almost as with a wing velocity normal to the wing.
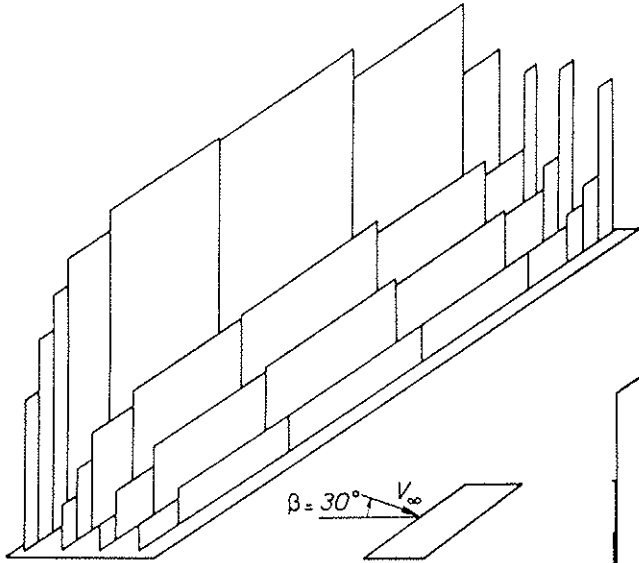
Fig. 13 — Rectangular wing in skewed flow. $\beta = 30°$.
Stationary case.
The geometric incidence is constant along the wing span.
The lifting segments location is given in figure 12a.
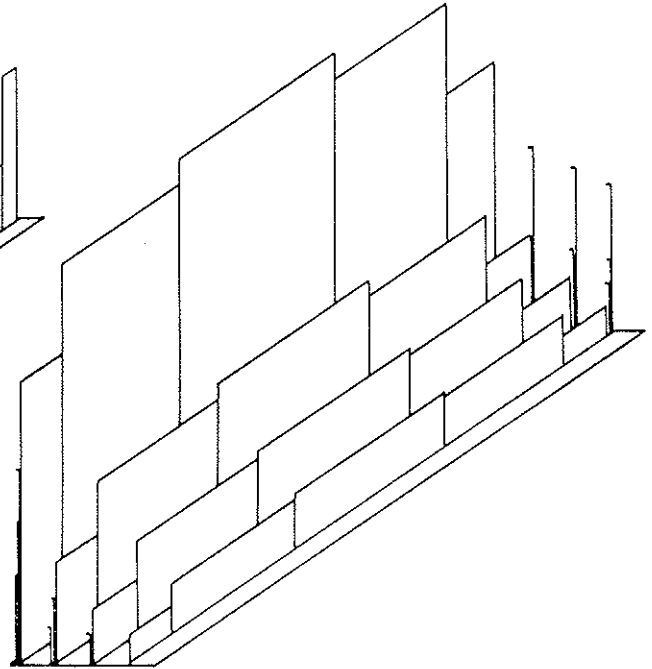
Fig. 14 — Rectangular wing in skewed flow, $\beta = 1°$.
Stationary case.

Figure 15 showns results obtained for the wing at $\beta = 30°$ and a oscillating movement around an axis at the 25 % chord position. The reduced frequency of the movement is $k = 0.04$. The real part (fig. 15a) looks like the ones obtained for $k = 0$ (fig. 13). For the imaginary part (fig. 15b) the first lifting line presents negative values of the lift which are usual at such low reduced frequencies. These negative values are smaller at the leading wing tip, making the phase angle between the force and the wing oscillating movement to vary along the wing span.
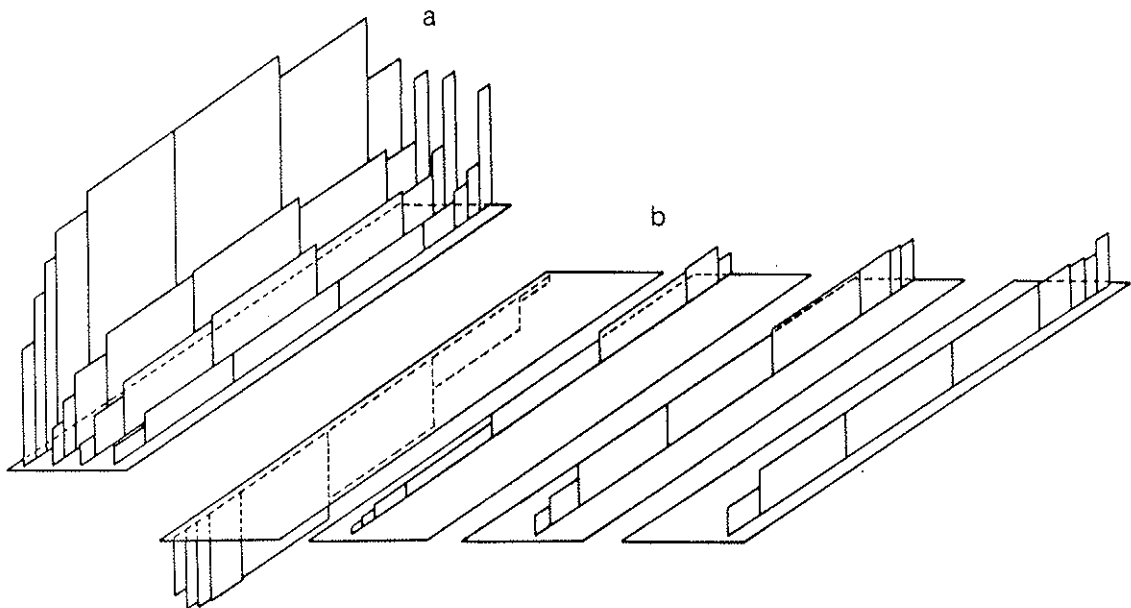
Fig. 15 — Rectangular wing in skewed flow, $\beta = 30°$. Reduced frequency k = 0.04
a) real part,
b) imaginary part. Scale multiplied by 10.
To make them easier to understand, the lifting lines have been represented on separate drawings.

V. CONCLUSION

The acceleration potential theory applied to numerical computation with a lifting line method has proved to be very successful in helicopter computations. The approximation of the helicopter blade with a single lifting line is not a limitation for the prediction of unsteady effects at the low reduced frequencies considered. Nevertheless, 3-D effects at the tip of the advancing blade are a limitation for the validity of the method. For a simpler case, the rectangular wing in a skewed flow, an approximate theory has been developed and some interesting effects shown to occur. The leading tip of the wing behaves as a kind of leading edge and the phase angle between the lifting force and the wing movement varies along the blade span.

ANNEX A

FOURIER TRANSFORM OF $H(\tau)$

The constants A, B, C, D are introduced; they are given by the formulas :

$$A = V_x^2 + \alpha V_y^2$$

$$B = -2 V_x (x-\eta) - 2\alpha V_y (y-c)$$

$$C = (x-\eta)^2 + \alpha (y-c)^2$$

$$D^2 = \frac{4 AC - B^2}{4 A^2} \qquad D > 0$$

the Fourier transform of $H(\tau)$ can be writen on the following form :

$$(A\text{-}1) \qquad J(\nu) = \frac{1}{A} \int_{-\infty}^{0} \frac{e^{j\nu\tau} \, d\tau}{\left[\tau + \frac{B}{2A}\right]^2 + D^2}$$

with the new variable $x = -\nu \left[\tau + \frac{B}{2A}\right]$, $J(\nu)$ becomes :

$$(A\text{-}2) \qquad J(\nu) = \frac{e^{-j\frac{\nu B}{2A}}}{2 AD} \left[\int_{-\frac{\nu B}{2A}}^{+\infty} \frac{e^{-jx} \, dx}{\nu D + jx} + \int_{-\frac{\nu B}{2A}}^{+\infty} \frac{e^{-jx} \, dx}{\nu D - jx} \right]$$

the formula (A-2) may be integrated in the complex plane making $Z = y + jx$, $J(\nu)$ is given by :

$$A.3 \qquad J(\nu) = \frac{e^{-j\frac{\nu B}{2A}}}{2AD} \left[-j\, e^{\nu D} \int_{\mathcal{C}_1} \frac{e^{-z}}{z}\, dz \;+\; j\, e^{-\nu D} \int_{\mathcal{C}_2} \frac{e^{-z}}{z}\, dz \right]$$

The paths of integration $\mathcal{C}_1$ and $\mathcal{C}_2$ are given in figure 16.
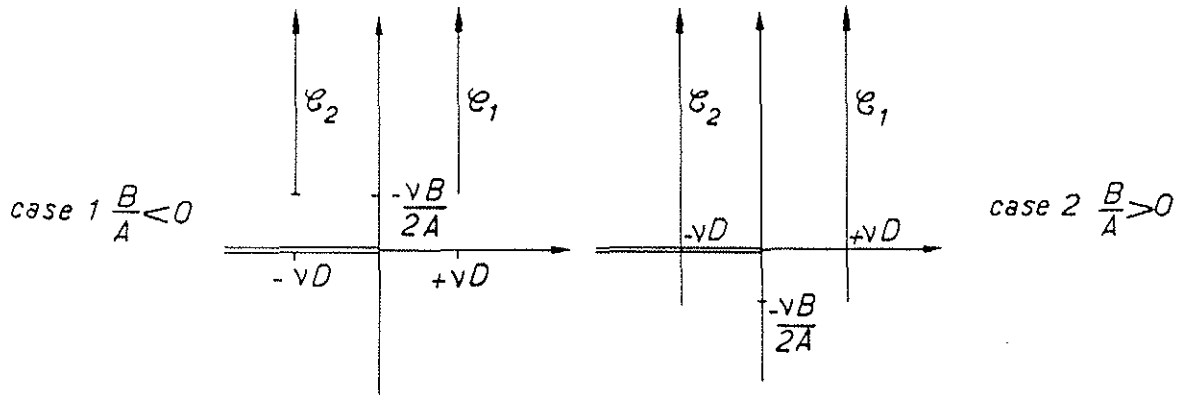
Fig. 16 — Paths of integration of $J(\nu)$.

Two different cases must be considered depending if $\mathcal{C}_2$ intersects the axis of negative abscissa or not.

$$\text{Taking} \qquad E_1(z) = \int_z^\infty \frac{e^{-t}}{t}\, dt$$

t is a complex number
and with $\quad C_1(z) = e^z E_1(z)$

in case 1 when $\frac{B}{A} < 0$ the path $\mathcal{C}_2$ does not cross the axis of $x < 0$ and $J(\nu)$ is given by :

$$J(\nu) = \frac{1}{2AD} \left[j\, C_1\!\left(-\nu D - j\frac{\nu B}{2A}\right) - j\, C_1\!\left(\nu D - j\frac{\nu B}{2A}\right) \right] \qquad \text{with} \quad \frac{B}{A} < 0$$

in case 2 when $\frac{B}{A} > 0$ the path $\mathcal{C}_2$ crosses the axis of negative abscissa. With the limit values of $E_1(z)$ given by

$$E_1\!\left(-\nu D - j0\right) = +j\pi$$

$$E_1\!\left(-\nu D + j0\right) = -j\pi$$

the value of $J(\nu)$ is given by :

$$J(\nu) = \frac{1}{2AD} \left[j\, C_1\!\left(-\nu D - j\frac{\nu B}{2A}\right) + 2\pi\, e^{\left(-\nu D - j\frac{\nu B}{2A}\right)} - j\, C_1\!\left(\nu D - j\frac{\nu B}{2A}\right) \right]$$

the function $C_1(z)$ is tabulated in many computers (see [9]).

REFERENCES

1. DAT R. *"Representation d'une ligne portante animée d'un mouvement vibratoire par une ligne de doublets d'accélérations".* La Recherche Aérospatiale, No. 133, Nov.-Dec. 1969. English translation NASA TTF 12952 (1970).

2. DAT R. *"La théorie de la surface portante appliquée à l'aile fixe et à l'hélice".* La Recherche Aérospatiale, No. 1973-4. English translation ESRO-TT.90 (1974).

3. COSTES J.J. *"Calcul des forces aérodynamiques instationnaires sur les pales d'un rotor d'hélicoptère".* La Recherche Aérospatiale, No. 1972-2. English translation NASA-TT.F15039 (1973). See also AGARD Report No. 595.

4. TRAN Cam Thuy, RENAUD J. *"Theoretical predictions of aerodynamic and dynamic phenomena on helicopter rotors in forward flight".* First European Rotorcraft and Powered Lift Aircraft Forum, 22-24 Sept. 1975. To appear in Vertica.

5. Von HOLTEN Th. *"On the validity of lifting line concepts in rotor analysis".* Vertica, vol. 1, No. 3, 1977.

6. BISPLINGHOFF R.L., ASHLEY H., HOFFMAN R.L. *"Aeroelasticity".* Addison-Wesley 1957.

7. BRIGHAM E.O.*"The Fast Fourier Transform".* Prentice Hall 1974.

8. DWIGHT, H.B. *"Tables of integrals and other mathematical data".* MacMillan 1961.

9. *"Handbook of Mathematical Functions with Formulas, Graphs and Mathematical Tables".* US Department of Commerce 1972.

▲▼▲